Journal of Molecular Liquids 412 (2024) 125814

Contents lists available at ScienceDirect

Journal of Molecular Liquids

journal homepage: www.elsevier.com/locate/molliq

A green approach to synthesize polybutene lubricants from mixed C4 monomers using supported dendritic ionic liquids

Amirhossein Ghavampoor [a], Naeimeh Bahri-Laleh [a,b,c,*], Samahe Sadjadi [a,**], Mehdi Nekoomanesh [a], Amir Vahid [d], Josep Duran [e], Maciej Spiegel [e,f], Albert Poater [e,**]

[a] Iran Polymer and Petrochemical Institute, P.O. Box 14965-115, Tehran, Iran
[b] RIKEN Center for Emergent Matter Science (CEMS), Saitama 351-0198, Japan
[c] Institute for Sustainability with Knotted Chiral Meta Matter (WPI-SKCM^2), Hiroshima University, Hiroshima 739-8526, Japan
[d] Research Institute of Petroleum Industry (RIPI), Tehran, Iran
[e] Institut de Química Computacional i Catàlisi and Departament de Química, Universitat de Girona, c/Maria Aurèlia Capmany 69, 17003 Girona, Catalonia, Spain
[f] Department of Organic Chemistry and Pharmaceutical Technology, Faculty of Pharmacy, Wroclaw Medical University, Borowska 211A, 50-556 Wroclaw, Poland

ARTICLE INFO

Keywords:
Polybutenes
Cationic polymerization
Catalyst
Oil

ABSTRACT

Lubricants, composed of a base oil and various additives, reduce friction and abrasion between moving surfaces. High-performance lubricants, especially in the automotive and space industries, have driven advancements in synthetic oils like polyalphaolefins (PAOs), known for their high viscosity index and stability. Low molecular weight polyisobutylenes (PIBs) are used in multiple applications, including as viscosity improvers. PIBs are produced via cationic polymerization of isobutylene using Lewis acid initiators and co-initiators, often conducted at low temperatures with harmful substances like BF_3. Efforts are being made to develop more eco-friendly processes, such as using $AlCl_3$ and ionic liquids (ILs). In this research, boehmite-supported dendritic ILs (Gen1 and Gen2) were synthesized and tested as co-initiators in Raffinate-1 polymerization. The ILs improved the stability of the catalytic system, allowing for reduced $AlCl_3$ usage, and produced PIBs with desirable molecular weight and viscosity characteristics. Density Functional Theory calculations unveiled the importance of the interaction of $AlCl_3$ with the ionic liquids.

1. Introduction

Lubricants are utilized as thin layers with low shear resistance between moving surfaces to reduce friction and abrasion [1,2]. They consist of a base oil (mineral, synthetic, or vegetable) and various additives. These additives enhance the lubricants' effectiveness and lifespan while improving their resistance to corrosion, oxidation, and temperature variations [3]. The quest for high-performance lubricants, capable of withstanding extreme temperatures and pressures [4,5], particularly in the space and automotive industries, has driven advancements in synthetic lubricants. These lubricants are designed to retain their properties at high temperatures without decomposing, combusting, or undergoing chemical degradation [4,6]. Lubricants must be viscous enough to provide adequate lubrication at high temperatures without causing engine damage, but not so viscous that they induce viscous friction at low temperatures. Polyalphaolefin (PAO) lubricants are widely recognized as the leading type of synthetic oil used in automotive and high-performance engine oil applications [7,8].

Polyalphaolefins (PAOs) are considered excellent for engine oil applications due to their non-polar nature, high viscosity index (>130), strong oxidation stability, low pour point, and compatibility with mineral oils [9,10]. These properties make them suitable for both low- and high-temperature conditions. One notable subgroup of PAOs is polybutenes (PB), which are of significant interest.

Low molecular weight polyisobutylenes (PIB) or polybutenes are used in various applications, including base oils, compressor oils, sealants, adhesive components, tackifiers in plastic film manufacturing, and viscosity improvers in oil formulations. Low molecular weight PIB (Mn = 500–5000 g mol^{-1}) is the most commercially significant class of isobutylene (IB) polymers, accounting for 75–80 % of the PIB market [11].

When C4 hydrocarbon streams, such as Raffinate-1, concentrated

* Corresponding author at: Iran Polymer and Petrochemical Institute, P.O. Box 14965-115, Tehran, Iran.
** Corresponding authors.
E-mail addresses: nbahri@hiroshima-u.ac.jp (N. Bahri-Laleh), s.sadjadi@ippi.ac.ir (S. Sadjadi), albert.poater@udg.edu (A. Poater).

https://doi.org/10.1016/j.molliq.2024.125814
Received 15 July 2024; Received in revised form 14 August 2024; Accepted 18 August 2024
Available online 19 August 2024

isobutylene, or dehydro effluent, are used, the resulting copolymer is known as PB. However, the polymer formed from pure isobutylene feedstock is also referred to as polyisobutylene [12]. Due to the minimal difference in boiling points between isobutylene and other C4 isomers, they cannot be separated by distillation [13,14].

Polyisobutylenes (PIBs) are a type of vinyl polymer produced through the cationic polymerization of isobutylene (IB) monomers. This process involves the use of Lewis acid initiators, such as boron trifluoride (BF_3), aluminum chloride ($AlCl_3$), and titanium tetrachloride ($TiCl_4$) [15,16].

In addition to the cationic initiator, a second chemical species known as a co-initiator is typically employed [17]. This co-initiator aids in the chain initiation step by forming an initiator/co-initiator complex that subsequently releases H^+ or R^+ (where R is an alkyl group) ions, which act as the primary initiators [18]. Furthermore, the co-initiator serves as a counter-ion at the active site during propagation, modifying the polymer chain's microstructure by donating electrons to the initiator [19]. Common co-initiators in cationic polymerization include various Lewis bases such as alcohols, water, and organic acids [20]. Among these, BF_3/co-initiator systems are frequently used in industrial PIB production [20]. However, this process is usually conducted at low temperatures, which is costly and impacts the safety and economics of isobutylene polymerization. Consequently, there is growing interest in raising the polymerization temperature to room temperature and substituting the toxic BF_3 with the less hazardous $AlCl_3$ to create a more environmentally friendly process [20,21]. Currently, two types of low molecular weight PIBs are available on the market, distinguished by their terminal olefinic groups: conventional polyisobutylene (C-PIB), primarily composed of *exo*-olefin terminal groups (>75 %) [15,22], and highly reactive polyisobutylene (HR-PIB), which mostly consists of less reactive tri- and tetra-substituted olefinic end groups. Additionally, it has been demonstrated that ionic liquid (IL) compounds can promote a greener process by reducing the amount of highly corrosive initiator required for the cationic polymerization of α-olefins when used in combination with $AlCl_3$ initiator [23,24,25]. ILs, which are organic salts with low melting points and vapor pressures [26,27], typically contain heterocyclic cations such as imidazolium or quaternary ammonium, while their anions can be various organic or inorganic compounds [28,29].

Ionic liquids (ILs) possess excellent properties such as tunable polarities, low toxicity, high thermal stability, non-flammability, and adjustable solvation, expanding their applications across various fields, particularly in catalysis [27,30,31]. Immobilized ILs are often used to create heterogeneous catalysts, enhancing catalytic activity and recyclability. For C4 based monomers, imidazole based ILs were extensively employed to prepare highly reactive PIB [32,33], and conventional PB [34]. In most of the studied systems, ILs facilitate polymer synthesis under relatively mild reaction conditions, i.e. close to room temperature and atmospheric pressure [35]. It is suggested that IL precursors, by poisoning certain active sites, produce polymers with narrow molecular weight distributions and more uniform chain topologies [25]. Depending on the ionic part environment, both increases [23] and decreases [33] in the molar mass of the final polybutenes were reported.

Based on the impressive results from using ILs and supported ionic liquids (SILs) in the polymerization of alpha-olefins [28,36,37] and also isobutylene [29], this research aims to design and apply new initiating systems based on $AlCl_3$ and two types of boehmite (B)-supported ILs with dendritic structures to polymerize Raffinate-1 and obtain conventional grade polyisobutylene, with the assistance of density functional theory (DFT) with characterization and predictive calculations [38,39,40]. These ILs can reduce the amount of $AlCl_3$ required for polyisobutylene polymerization. The dendritic structure of SILs allows for more active sites, beneficial for the stabilization of the carbenium ion.

2. Experimental

2.1. Materials

The following solvents and reagents were used to synthesize SILs: boehmite, trichloro triazine, (3-aminopropyl) triethoxysilane (APTES), 2,4,6-trichloro-1,3,5-triazine (TCT), piperazine, tetrahydrofuran, dimethyl sulfoxide, toluene, and chlorosulfuric acid, all sourced from Sigma-Aldrich. Additionally, anhydrous $AlCl_3$ (99.9 %), NaOH, and ethanol, used in the polymerization step, were also obtained from Sigma-Aldrich. Raffinate-1 (containing 50 % isobutylene monomer) was generously donated by Shazand Petrochemical Company, Arak, Iran.

2.2. Instruments

To confirm the formation of dendritic IL on the boehmite support, Fourier transform infrared (FTIR) spectra of the SILs and boehmite were recorded using a PERKIN-ELMER Spectrum 65 with KBr pellets. The weight percent loading of ILs on boehmite was assessed via thermogravimetric analysis (TGA) with a METTLER TOLEDO apparatus (heating rate of 10 °C/min under O_2 atmosphere). The morphology of the SIL and the homogeneous dispersion of ILs onto the boehmite were evaluated through SEM and elemental mapping analysis using a MIRA 3 TESCAN-XMU instrument.

X-ray diffraction (XRD) patterns of the SILs were recorded with a Siemens D5000 apparatus equipped with Cu Kα radiation. Gel permeation chromatography (GPC) was conducted using a GPC Agilent 1100 to obtain the molecular weights and polydispersity of the synthesized PBs, with PS standards calibrating molecular weight and THF as the solvent.

^{1}H NMR spectroscopy, performed with a Bruker DRX400MHz NMR spectrometer (at 25 °C) in deuterated chloroform ($CDCl_3$), was used to analyze the microstructure and composition of the olefin end groups, considering the chemical shift of $CDCl_3$ solvent ($\delta = 7.26$ ppm) as an internal standard.

^{13}C NMR spectroscopy was performed under fully H-decoupled conditions with the following parameters: delay time: 6 s, number of scans: 3000, pulse angle: 90°, PulProg: zgPg. The boiling point and carbon number of the synthesized PAOs were determined using an HT-CNS SimDis instrument (Agilent 7890 A gas chromatograph equipped with FID, NCD, and SCD, and AC Simulated Distillation Software) combined with a detailed hydrocarbon analyzer (DHA, Agilent 7890 A Gas Chromatograph with FID and AC DHA Software). The kinematic viscosity (KV) of the polymers at 40 and 100 °C were measured according to the ASTM D445 and ASTM D2270 standards, respectively. All viscosity measurements were conducted 5 times, and the average values are reported here.

2.3. Supported ionic liquids (SILs) synthesis

Two generations of dendritic SILs (Gen1 and Gen2) were developed in this research. The detailed synthetic procedures for these catalysts are as follows:

2.3.1. Synthesis of Gen1

The catalyst production process began with the functionalization of boehmite using APTES. Initially, boehmite (4.0 g) was suspended in dry toluene (90 ml), followed by the addition of APTES (4.0 ml). The reaction mixture was maintained at 110 °C for 24 h under a nitrogen atmosphere. Upon completion, the product was separated by centrifugation at 6000 rpm for five minutes and then dried at 110 °C for 24 h.

In the second step, TCT (2.48 g) was dissolved in dry THF (90 ml) and reacted with the product from the first step at 66 °C for 24 h under nitrogen. After the reaction, the solid was separated by centrifugation (5500 rpm for 6 min) and dried at 66 °C overnight.

The third step involved preparing a solution of piperazine (2.32 g) in dry DMSO (100 ml) and reacting it with the product from the second step for 24 h at 100 °C under nitrogen. The resulting solid was then separated by centrifugation (6000 rpm for 5 min) and dried at 150 °C overnight.

For the synthesis of Gen1, 1.57 g of the final product from the third step was reacted with chlorosulfuric acid (0.6 ml) at room temperature under a nitrogen atmosphere for 24 h. The solid product was separated by centrifugation (5500 rpm for 6 min), washed with DMSO, and dried at 80 °C overnight. See Scheme 1 for detailed information.

2.3.2. Synthesis of Gen2

In the initial stage, TCT (4.97 g) was suspended in dry THF (100 ml). Non-sulfonated Gen1 (3.5 g) was then reacted with the suspension at 60 °C for 24 h under a nitrogen atmosphere. After the reaction was complete, the solid was filtered off by centrifugation (6.0 min and 5500 rpm) and dried at 80 °C overnight.

In the next step, piperazine (4.65 g) was suspended in dry DMSO (130 ml). Then, the product of previous part was added and reacted with the suspension at 100 °C for 24 h under a nitrogen atmosphere. After completion, the solid was centrifuged twice (6 min at 6000 rpm), washed with DMSO, and dried at 80 °C for 24 h.

In the final step, chlorosulfuric acid (1 ml) was added to the second step's product and reacted with it at room temperature under a nitrogen atmosphere. At the end, the solid product was filtered off by centrifugation (6 min and 5500 rpm) and dried overnight at 80 °C. See Scheme 1 for detailed information.

2.3.3. Polybutene synthesis

Raffinate-1 was polymerized via a solution cationic polymerization route in a 2-L Butchi-type reactor at 30 °C for 30 min. Before each experiment, the reactor was purged with nitrogen gas for 20 min at room temperature. Next, 170 ml of hexane was added to the reactor as a solvent. Subsequently, 0.14 ml of ethanol and 120 g of Raffinate-1 were fed into the reactor. After the temperature of reactor's contents reached to 30 °C, a mixture of 1.68 g of $AlCl_3$ co-initiator and 0.72 g of either Gen1 or Gen2 dispersed in 10 mL of dichloromethane was added to the reactor using a feeding column. After stirring for 30 min while maintaining the temperature, the solution was discharged and washed three times with a 5 wt% NaOH solution using a decanter funnel. A rotary evaporator at 180 °C under a −0.7 bar vacuum was used to concentrate and purify the resulting PB by removing water, unreacted monomers, and excess solvent. Finally, 46 g of oil was obtained.

2.4. Computational details

The Gaussian 16 package was used for all DFT calculations [41]. Geometry optimizations were performed without symmetry constraints

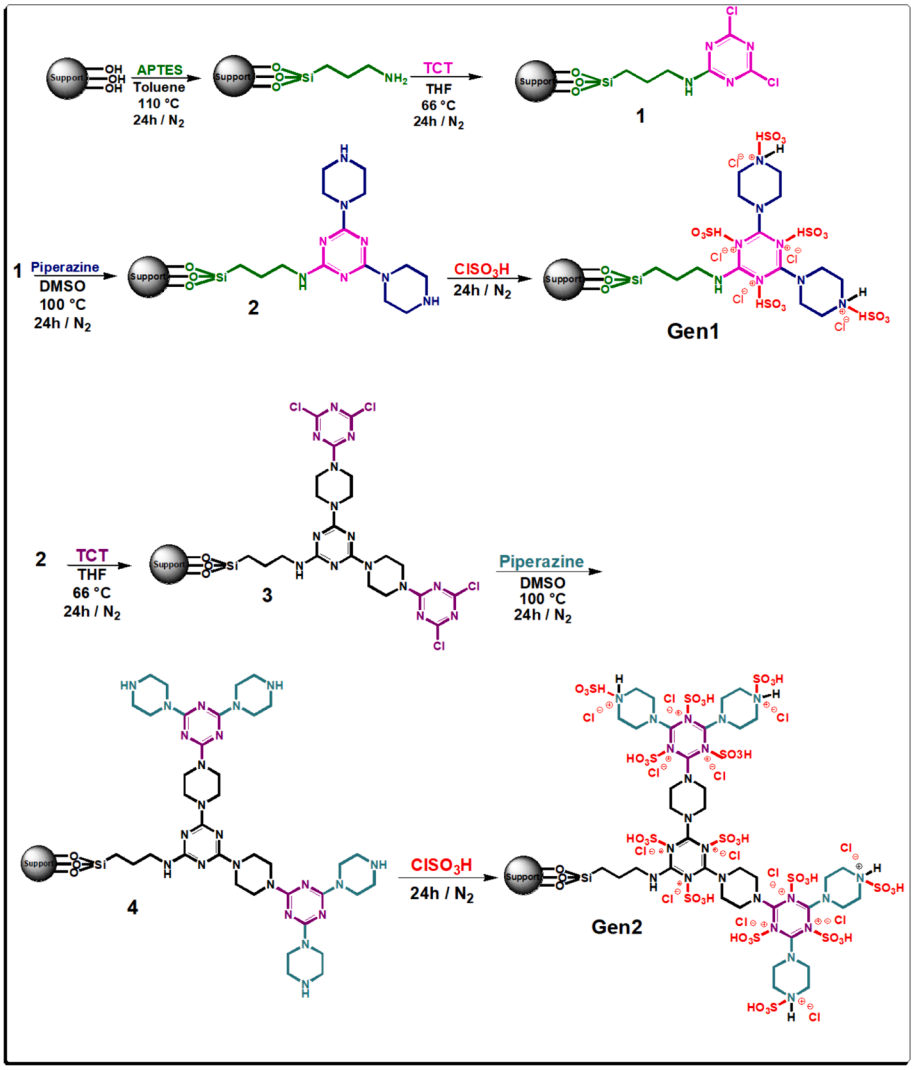

Scheme 1. Procedures for the synthesis of Gen1 and Gen2.

using the Becke and Perdew pure Generalized Gradient Approximation (GGA) functional, BP86 [42,43], along with dispersion corrections via the Grimme D3 method [44]. The split-valence basis set (Def2SVP keyword in Gaussian) was applied [45,46]. Analytical frequency calculations determined the nature of stationary points, whether minima or transition states. The Intrinsic Reaction Coordinate (IRC) procedure was employed to confirm and trace the minima connected by each transition state. Additionally, single-point energy calculations were conducted using the hybrid GGA functional B3LYP [47,48,49], and the def2TZVP basis set for all atoms [50]. The solvent effect was explicitly considered using the polarizable solvation model (SMD) with water as the solvent, following the variation of the Integral Equation Formalism Polarizable Continuum Model (IEFPCM) developed by Truhlar and co-workers [51]. In summary, the reported Gibbs energies incorporate energies obtained at the B3LYP-D3/def2TZVP(smd-H_2O)//BP86-D3/Def2SVP level of theory, corrected for zero-point energies, thermal corrections, and entropy effects, evaluated with the BP86-D3/Def2SVP method.

3. Results and discussion

3.1. B-ILs characterization

To accurately characterize the Boehmite supported ionic liquids (B-ILs), appropriate analyses encompassing TGA, FTIR, and SEM were considered. First, one beneficial approach to confirm the combination of ILs on the boehmite support is FTIR spectroscopy. It is a beneficial method to confirm the integration of ILs on the boehmite support. Initially, the structure of the ILs was assessed. FTIR spectra of boehmite, Gen1, and Gen2 are shown in Fig. 1. The boehmite structure's Al—O bond stretching vibrations caused some bands centered at 480, 630, and 740 cm^{-1} [34,52]. The bands at 1065 and 1160 cm^{-1} are ascribed to the symmetrical bending vibrations of hydrogen binding [53,54]. The shoulder at 1639 cm^{-1} is attributed to the bending mode of the absorbed water [55,56]. Bands that appeared in the range of 3089 and 3404 cm^{-1} are due to the stretching of —OH bonded to Al [49,51]. The —OH bound bands broadening in the Gen1 and Gen2 FTIR spectra indicated the formation of hydrogen bonds. For pure boehmite, the vibration band at about 1070 cm^{-1} is attributed to the bending vibration of deprotonated hydroxyl groups of Al—O, implying the tetrahedral symmetry structure of boehmite [57]. A strong band at 1696 cm^{-1} is related to the —C═N functionality of the TCT ring. The —CH bond characteristic bands appeared at 2936 and 2851 cm^{-1} (aliphatic C—H stretching) [58]. Typically, the band at 850 cm^{-1} is indicative of stretching vibration of C—Cl of TCT [54]. The disappearance of the C—Cl bond together with the N—H band of amines at about 1610 cm^{-1} in Fig. 1 confirms the formation of a C-N linkage by substitution of the amine group from piperazine [54]. The stretching vibration of Si—O is observed at 1115 cm^{-1} [59], these findings verified that boehmite has been successfully modified with an IL.

To investigate the loading of dendritic IL on boehmite, TG analysis of pure boehmite, Gen1 and Gen2 was performed, as shown in Fig. 2. The TG curve for boehmite exhibits two distinct weight loss stages. The first stage, occurring below 200 °C, is attributed to the evaporation of physically adsorbed water and solvent molecules present on the boehmite surface or within its interlayers. The second stage, which accounts for most of the mass loss, occurs between 300 and 520 °C due to the partial dehydroxylation of boehmite and its conversion to γ-alumina. In comparison to pure boehmite, the TG curves of Gen1 and Gen2 show an additional significant mass loss between 200 and 300 °C, which is attributed to the decomposition of the organic phase of the dendritic ILs. This additional weight loss was measured at 11.21 % for Gen1 and 14.17 % for Gen2, indicating the successful loading of ILs onto the boehmite support.

To verify the stability of the boehmite structure after grafting ILs, XRD analysis was employed on both pure boehmite and Gen1. As depicted in Fig. 3, the characteristic peaks of boehmite appeared at $2\theta =$ 14.1°, 28.1°, 38.4°, 49.1°, 55.6°, 65°, and 72.3°. These peaks are also observable in the XRD pattern of Gen1 without any displacement. This issue not only confirms the structural stability of boehmite upon grafting of dendritic IL, but also indicates that the IL formed did not penetrate within the interlayer space of boehmite but formed on its surface.

The possible morphological changes due to ionic liquid grafting onto boehmite were appraised by comparing SEM images of boehmite and Gen1 (Fig. 4a, b). Gen1 shows a non orthorhombic cubic morphology, distinct from the pristine boehmite, indicating that the introduction of ILs on the boehmite surface significantly alters its morphology. Specifically, the SEM images of B-ILs reveal small aggregates covering the boehmite orthorhombic cubes, rendering their surfaces rough.

To get further insight into the dispersion of the grafted IL onto the surface of boehmite, elemental mapping analysis was conducted. Fig. 5a and b show the detected elements in the supported ILs, including Al, O, C, N and Cl. From all the latter atoms, Al and O atoms are representative of the boehmite framework, whereas C, N and Cl are indicative of the attached IL on the pristine boehmite. As C, N and Cl atoms are uniformly dispersed on the boehmite support, it can be deduced that ILs were homogeneously grafted on the boehmite support.

3.2. Polybutenes characterization

The synthesized B-ILs, in combination with the $AlCl_3$ co-initiator,

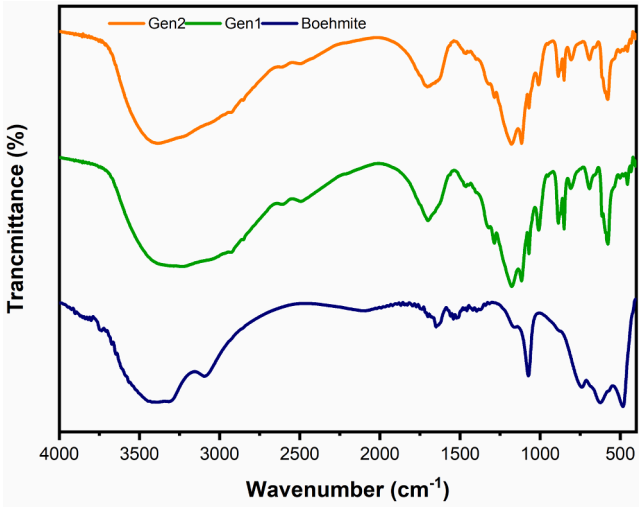

Fig. 1. FTIR spectra of pure boehmite, Gen1 and Gen2.

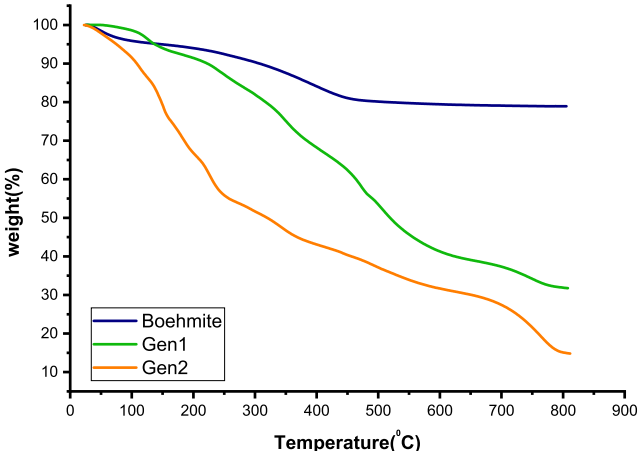

Fig. 2. Thermograms of pure boehmite, Gen1 and Gen2.

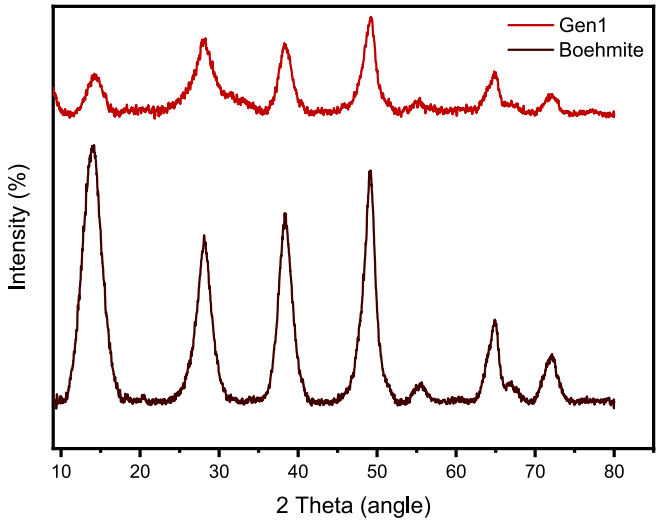

Fig. 3. XRD patterns of boehmite and Gen1.

were briefly tested in the cationic polymerization of mixed C4 monomers, commercially known as Raffinate-1. This was done to evaluate the feasibility of producing conventional grade PBs and to assess the reactivity of these systems. Neat $AlCl_3$ served as the blank system.

As previously noted, our research group successfully used ILs [28,32], and their supported counterparts [33] to prepare poly-alphaolefin lubricants with the desired molecular weight and microstructure [60]. Furthermore, ILs have proven useful in the synthesis of viscosity improvers [23] of the polyisobutylene type [61,62]. Building on these outstanding findings, we aimed to develop new B-ILs for the cationic polymerization of Raffinate-1 to produce low molecular weight polybutenes. To this aim, two different kinds of dendritic ILs supported on boehmite, Gen1 and Gen2, were tested here. A mixture of $AlCl_3$ and B-ILs was used in the polymerization tests. It is worth mentioning that in the case of using B-ILs, the combined weight of B-ILs and $AlCl_3$ was considered as the co-initiator dosage. The effects of designed B-ILs on the catalytic performance of $AlCl_3$/EtOH initiating system, average molecular weight, and dispersity index (Đ) of the produced copolymers were thoroughly studied. The results in Table 1 indicate that by employing $AlCl_3$/B-ILs/EtOH initiating/co-initiating systems for the cationic polymerization of Raffinate-1 does not significantly affect the yield. However, it allows for a reduction of up to 30 % in the dosage of corrosive $AlCl_3$. This reduction is advantageous for decreasing process risk in industrial plants.

The presence of B-ILs leads to a slight increase in the number average molecular weight (M_n) of the polybutenes. This is likely due to interactions between the B-ILs and the carbenium ion (C^+) on the developing chain. The ionic nature of ILs and the hydroxyl groups on the surface of boehmite are believed to stabilize the carbonium ion. Consequently, the catalytic system containing the synthesized B-ILs produces polybutenes with relatively high molar mass PBs.

The deconvolution of GPC curves was achieved with ORIGINPRO 2018, Graphing & Analysis software. The software's computation of the R Square, sometimes referred to as the coefficient of determination (COD) [48], exceeded 0.999 for every graph in every calculation. This high value ensures accurate estimations. Deconvolution of the GPC curves produced a weighted sum of three Gaussian distribution functions, as shown in Fig. 6, from which the quantity and productivity of each of the three active sites were determined. Using neat $AlCl_3$, PBs with different chain lengths were produced via 3 different active sites with M_n of 245, 251 and 235 g mol^{-1} possessing 47, 36, and 17 wt%, respectively. When Gen1 was included in the initiating system, the M_n of the copolymers produced by each active site experienced a significant escalation to 379, 361, and 406 g mol^{-1}. Gen2 provided even more stabilization for the carbenium ion than Gen1, resulting in further increases in the M_n of copolymers generated by each active site to 339, 328, and 353 g mol^{-1} with the inclusion of Gen2 in the composition of the initiating system. Using Gen2 instead of Gen1 results in an enhanced M_n, indicating that Gen2 has more stability for the carbenium ion. In total, the differences in steric hindrance and electronic characteristics of these B-ILs caused no significant changes in M_n, Đ, or the wt.% of the active sites.

VI, KV^{40} and KV^{100} are crucial characteristics for lubricants applications. Indeed, they should exhibit high VI values, which guarantee thick hydrodynamic film formation between applied surfaces at high temperature together with high flow ability performance, less resistance towards flow at low temperatures. In fact, VI characteristic is an indication of viscosity changes of a fluid as a function of temperature, so that the oil with high VI has minimal viscosity changes with temperature variation.

Kinematic vicosity and viscosity index were measured by capillary viscometer at 40 and 100 °C. Viscosity of all three samples has been reported in Table 1. There is a direct relationship between viscosity and molecular weight: as molecular weight increases, viscosity also enhances. It is generally accepted that the mobility of polymer chains becomes more difficult due to the increase in molecular weight. As a result, the sample synthesized using the initiator system includes $AlCl_3$/Gen2 has a higher viscosity compared to the other samples.

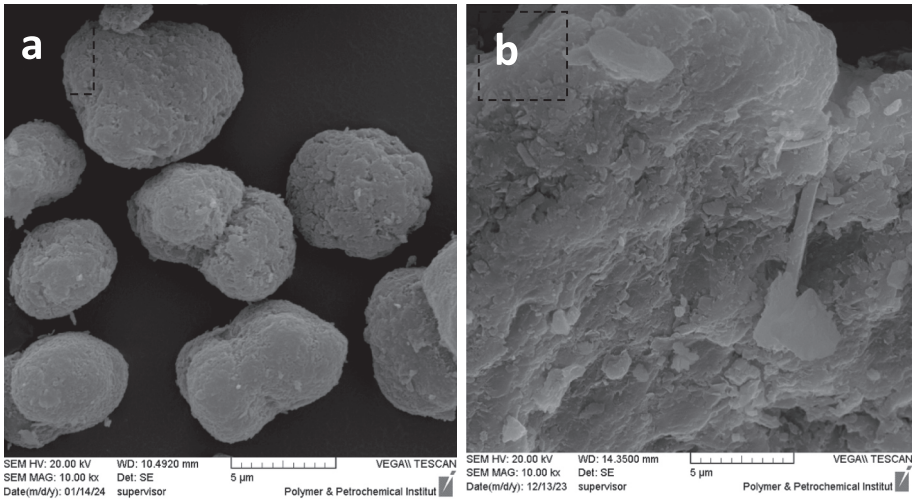

Fig. 4. SEM images of (a) boehmite and (b) Gen1.

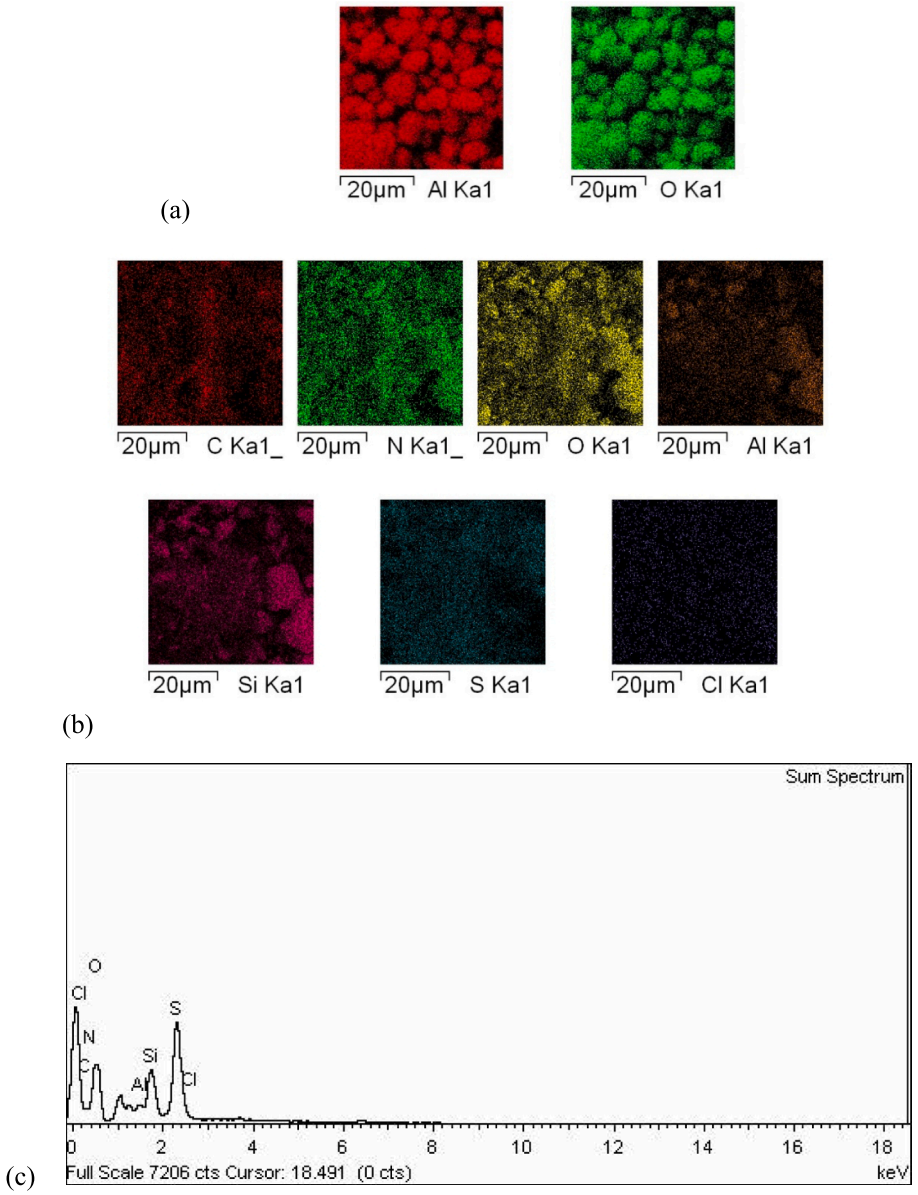

Fig. 5. Elemental mapping analysis of (a) boehmite and (b) Gen1, (c) EDX analysis of Gen1.

Table 1
Productivity of the employed catalysts and molecular weight and viscosity characteristic of the prepared PBs.[a]

Entry	Co-initiator	Yield (%)[b]	KV_{40} (cSt)	KV_{100} (cSt)	VI	M_n (g/mol)	Đ
1	$AlCl_3$	78	34.4	7	148	481	1.91
2	$AlCl_3$/Gen1	75	70	11.4	135	528	1.95
3	$AlCl_3$/Gen2	75	78.6	13.3	141	541	1.73

[a] Polymerization conditions: Raffinate-1 = 120 g, Initiator: EtOH, EtOH/$AlCl_3$ = 0.5 mol/mol, Co-initiator ($AlCl_3$ + Ionic liquid) = 2.4 g, T = 30 °C, t = 30 min, P = 2.6 bar.

[b] Yields are calculated based on isobutylene content.

Another distinguishing feature of polybutenes is the composition of olefin groups. Due to the mechanism and nature of alkene polymerizations, transfer reactions cause that the resulted polymer contains a single double bond in each chain. The position of this double bond is therefore a critical property of the product. Highly reactive polyisobutylene (HR-PIB) and conventional polyisobutylene (C-PIB) are the two grades of polyisobutylene. HR-PIB is principally composed of double bonds located at the terminal (vinylidene) position, whereas double bonds in C-PIB are generally internal-the sum of *tri*-substituted, *tetra*-substituted, coupled, and endo olefins (see Fig. S1). Exo-olefins, also known as vinylidene, are substantially more reactive than internal olefins. The lower *exo*-olefin end group content is favorable for conventional grade PB, since it improves the thermal oxidative stability of the polymer for high temperature uses [63]. Consequently, the lower the content of *exo*-olefins in conventional-grade PIBs or PBs, the higher their thermal stability in high temperature applications.

Hence, to assess the characteristics of these double bonds, ^{1}H NMR spectroscopy was employed focusing on the δ = 2.75–5.70 ppm region. According to the ^{1}H NMR spectra of Fig. 7 and the summarized results in Table 2, polybutenes obtained via neat $AlCl_3$ contain a total *exo*-olefin end group content of 4.33 %. Nevertheless, unde the same reaction conditions, co-initiator systems containing B-ILs increased the total *exo*-olefin groups to 9.51 % and 5.88 % for the $AlCl_3$/Gen1 and $AlCl_3$/Gen2 systems, respectively. It is worth noting that in conventional grade

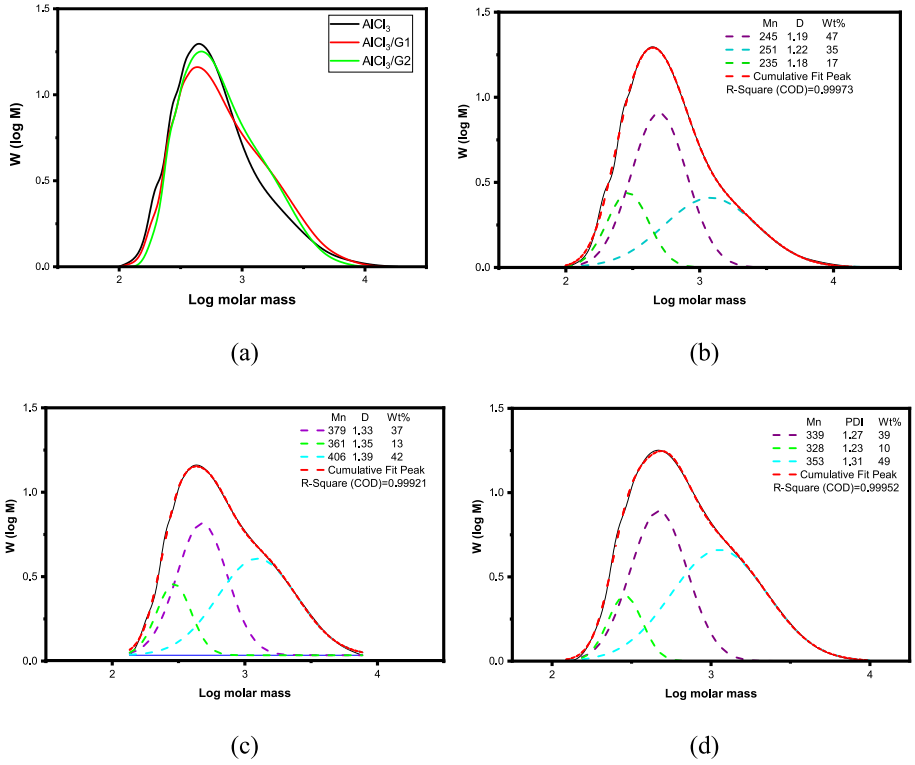

Fig. 6. (a) GPC curves of obtained PBs using 2 types of co-initiating systems, and the deconvolution of the GPC curves to a weighted summation of 3 lognormal distribution functions for PBs from (b) neat $AlCl_3$, (c) $AlCl_3$/Gen1, (d) $AlCl_3$/Gen2 systems. The features of each distribution such as M_n, dispersity index and weight fraction are included in the plots.

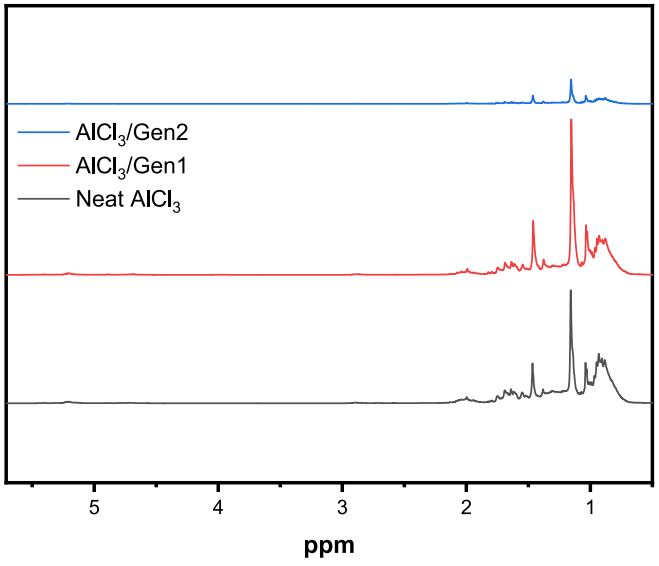

Fig. 7. ^{1} HNMR spectra of the obtained PBs employing, neat $AlCl_3$, $AlCl_3$/Gen1, $AlCl_3$/Gen2 systems.

Table 2
End group distribution of the synthesized PBs using B-ILs and neat $AlCl_3$.

Run	Exo (4.66)	Endo (5.17)	Tri (5.19)	Tetra (2.87)	Coupled (4.83–4.85)
$AlCl_3$	4.33	40.09	26.04	22.65	7.36
$AlCl_3$/Gen1	9.51	34.1	26.61	24.42	7.57
$AlCl_3$/Gen2	5.88	31.37	30.88	24.50	7.35

polybutenes, lower *exo*-olefin content correlates with higher thermal stability. The results indicate that the AlCl3/Gen1 system promotes more transfer reactions compared to the $AlCl_3$/Gen2 system. Additionally, during the hydrogenation step, typically conducted after the polymerization process, all C═C bonds are saturated to ensure the high stability of the final oil.

To assess the microstructure of PB copolymers, ^{13}C NMR spectroscopy was also performed. The ^{13}C NMR spectra for the copolymers generated from the neat $AlCl_3$, $AlCl_3$/Gen1, and $AlCl_3$/Gen2 catalytic systems are shown in Fig. 8, in a zoom view within the 7–62 ppm range. Considering the polymerizable monomers in Raffinate-1 (isobutene, 1-butene, cis- and trans-2-butene), and the position of each of carbon in the chain, chemical shifts may vary, leading to the appearance of additional peaks. A thorough assignment of the different carbon atoms was carried out in accordance with the literature [64,65]. Table 3 summarizes the ^{13}C NMR spectra data for the studied catalytic systems. According to Table 3, IB (isobutylene) units had a contribution of about 70.44–79.80 % in the chains across all catalytic systems. The most significant contribution was related to $AlCl_3$/Gen2 system, whereas neat $AlCl_3$ caused the least participant of 72.44 % for IB units. It means that both synthesized B-ILs slightly increase the IB percentage along the length of the chain. The rationalization of such enhancement is still unclear. Following the mechanism proposed recently by some of us [34], the cationic polymerization of C4 monomers consists of three major steps: 1) initiation stage which comprises of two steps, i.e. complexation of aluminum chloride with ethanol that leads to the formation of initiator–coinitiator complex CH3CH2(AlCl3OH) and reaction of the first monomer with the so-called complex; 2) propagation step proceeds by adding subsequent monomers to the carbocation section; 3) transfer/termination stage. It is speculated that ILs interact with carbocation parts in all three steps.

Simulated distillation (SimDis) curves of the analyzed PBs were examined (Fig. 9) using a high-performance capillary gas chromatograph and simulation distillation software. The obtained data indicated

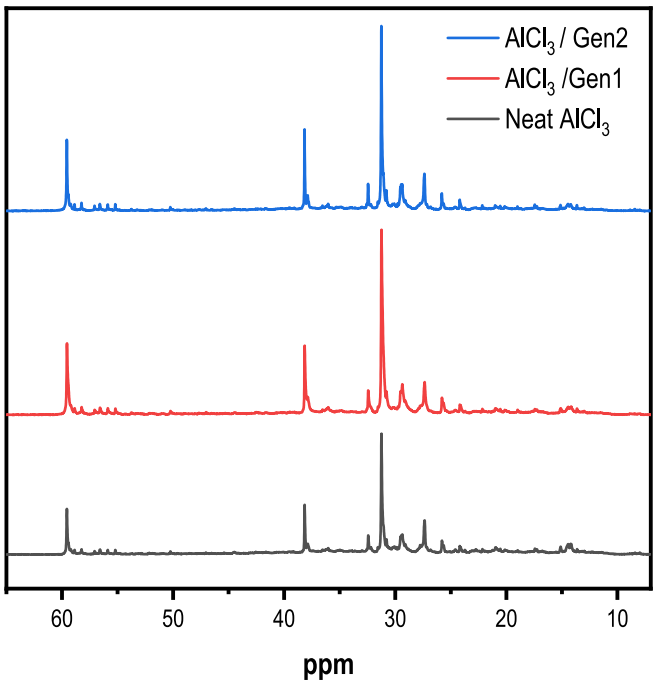

Fig. 8. Aliphatic region in the ^{13}C NMR spectra of PB copolymer synthesized via $AlCl_3$, $AlCl_3$/Gen1 and $AlCl_3$/Gen2 system.

Table 3
The share of the Raffinate-1 monomers, isobutene, 1-Bu, *cis*- and *trans*-2-Bu, in the prepared PB chains using studied catalytic systems, obtained from ^{13}CNMR spectra.

Run	IB (%)	1-Bu, *cis*- and *trans*-2-Bu
$AlCl_3$	72.44	27.56
$AlCl_3$/Gen1	77.97	22.03
$AlCl_3$/Gen2	79.80	20.20

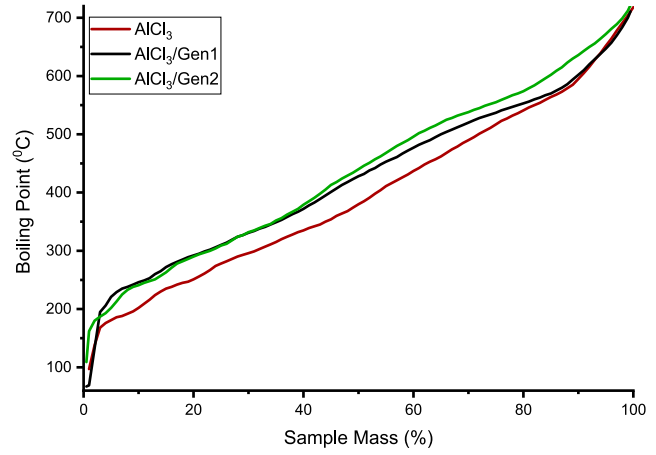

Fig. 9. SimDis curves of the synthesized PBs.

that the as-prepared PBs exhibited almost a broad peak that can contain several tiny sharp peaks. Additionally, the deep analysis of the SimDis curves is presented in Table 4, including the temperatures at which 10, 50, and 90 % of PB evaporate (abbreviated as T10, T50, and T90, respectively), as well as the synthesized PBs' starting and ultimate boiling points. The initial boiling points were measured at 97, 67 and 109 °C for samples produced with neat $AlCl_3$, $AlCl_3$/Gen1 and $AlCl_3$/Gen2, respectively. Notably, due to its large molecular weight, the

Table 4
Initial and final boiling points, T_{10}, T_{50}, and T_{90} of the synthesized PBs, derived from SimDis analysis.

Run	iBP	fBP	T_{10}	T_{50}	T_{90}
$AlCl_3$	97	724	209	385	605
$AlCl_3$/Gen1	67	711	246	428	602
$AlCl_3$/Gen2	109	722	241	440	636

sample produced using $AlCl_3$/Gen2 exhibited the highest boiling point, and the sample synthesized by neat $AlCl_3$ showed the lowest boiling point. Furthermore, the trend observed in T_{10}, T_{50}, and T_{90} closely mirrored the trend observed in the M_n data trend from the GPC curves.

3.3. Computational characterization

To gain a better understanding of the structure, DFT calculations were performed. The Gen1 and Gen2 structures were optimized, followed by an investigation of the optimal insertion site for $AlCl_3$. As expected for this type of interaction with ionic liquids, the binding with chlorides leading to $AlCl_4^-$ results in a binding energy of 45.7 kcal/mol. However, this variant would hinder subsequent polymerization activity. In contrast, interaction with a nitrogen atom of the triaza aryl ring stabilizes the system by 24.4 kcal/mol, and interaction through the outermost oxygen of an SO_3 group results in stabilization of 20.6 kcal/mol. Additionally, an exhaustive analysis was conducted for all positions in Gen1, revealing the positive outcome that regardless of where $AlCl_3$ positions itself, the process is exergonic, with a minimum energy release of 9.9 kcal/mol.

The disparity in binding energies of $AlCl_3$ must have a structural or electronic origin. In the first case, considering the strength of the aluminum bond with the coordinating atom based on the Mayer Bond Order (MBO) approach, values range from 0.757 with the Cl anion to a notably lower 0.581 for the least favored coordination, though still favored as previously mentioned. Intermediate values include 0.944 for binding with the N of the ring and a drastic reduction to 0.535 for the oxygen of the SO_3 group. Tracking the remaining values (see Table S1) indicates no linear relationship between bond strength and binding energy, although there is a discernible trend. Expanding the scope to the entire sphere occupied by aluminum, using the $\%V_{Bur}$ and steric maps by Cavallo and collaborators [66,67,68], reveals values of only 24.5 % for $AlCl_4^-$, while 31.3 % and 26.2 % through N or O, respectively. A deeper analysis through the quadrants shows no clear correlation between the most or least hindered quadrants and binding energy [69,70,71]. Shifting the focus to Natural Population Analysis (NPA) charges, aluminum has a charge of 1.500 through N and 1.492 through O, indicating a negligible difference. For $AlCl_4^-$, the charge significantly drops to 1.356 because Cl donates electronic density to the metal, retaining a charge of only −0.570. These values are almost identical to those of isolated $AlCl_4^-$, which are 1.352 and −0.588, respectively. Ultimately, weak interactions generated by $AlCl_3$ at each coordination site must be considered. Figs. 10 and 11, with non-covalent interaction (NCI) plots [72,73,74], reveal the contributive strength of surrounding atoms for the $AlCl_4^-$ case [23,75], which stands out as an outlier, as well as for coordination with N or any other position [76,77]. These observations are further stressed out in the framework of Bader's Atoms-in-Molecules analysis depicted in Figs. S1 and S2.

4. Conclusions

The synthesis and characterization of lubricants, particularly polyisobutylenes (PIBs) and polybutenes (PBs), highlight significant advancements in the field, driven by the need for high-performance lubricants capable of withstanding extreme conditions in industries such as automotive and aerospace. This study explored the creation of boehmite-supported ionic liquids (B-ILs) with dendritic structures,

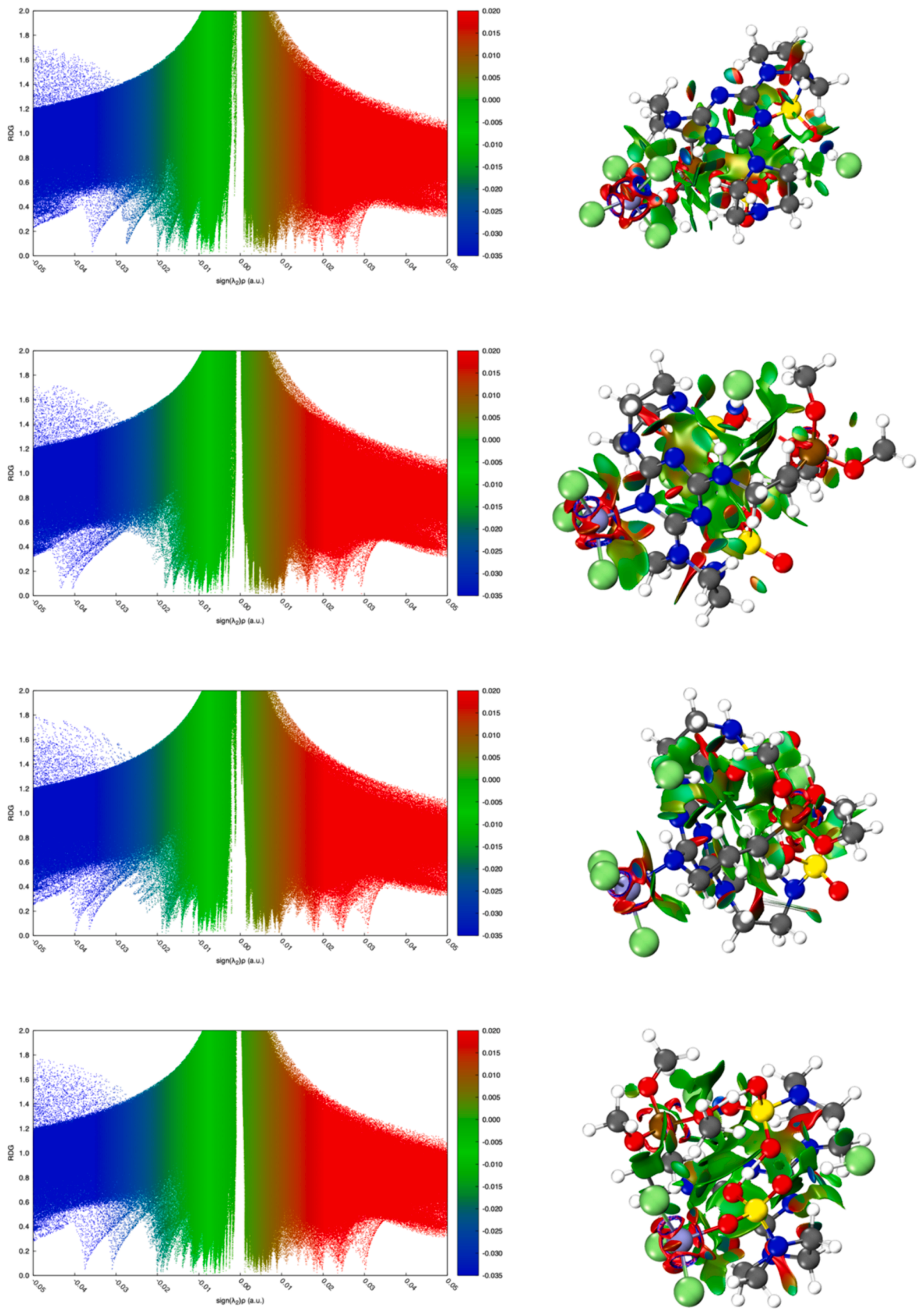

Fig. 10. 2D (left) and 3D (right) NCI plots of Gen1 and the addition of $AlCl_3$ on (a) Cl, (b) N of the aromatic ring, (c) non-aromatic N, and (d) the most accessible O atom of a SO_3 group.

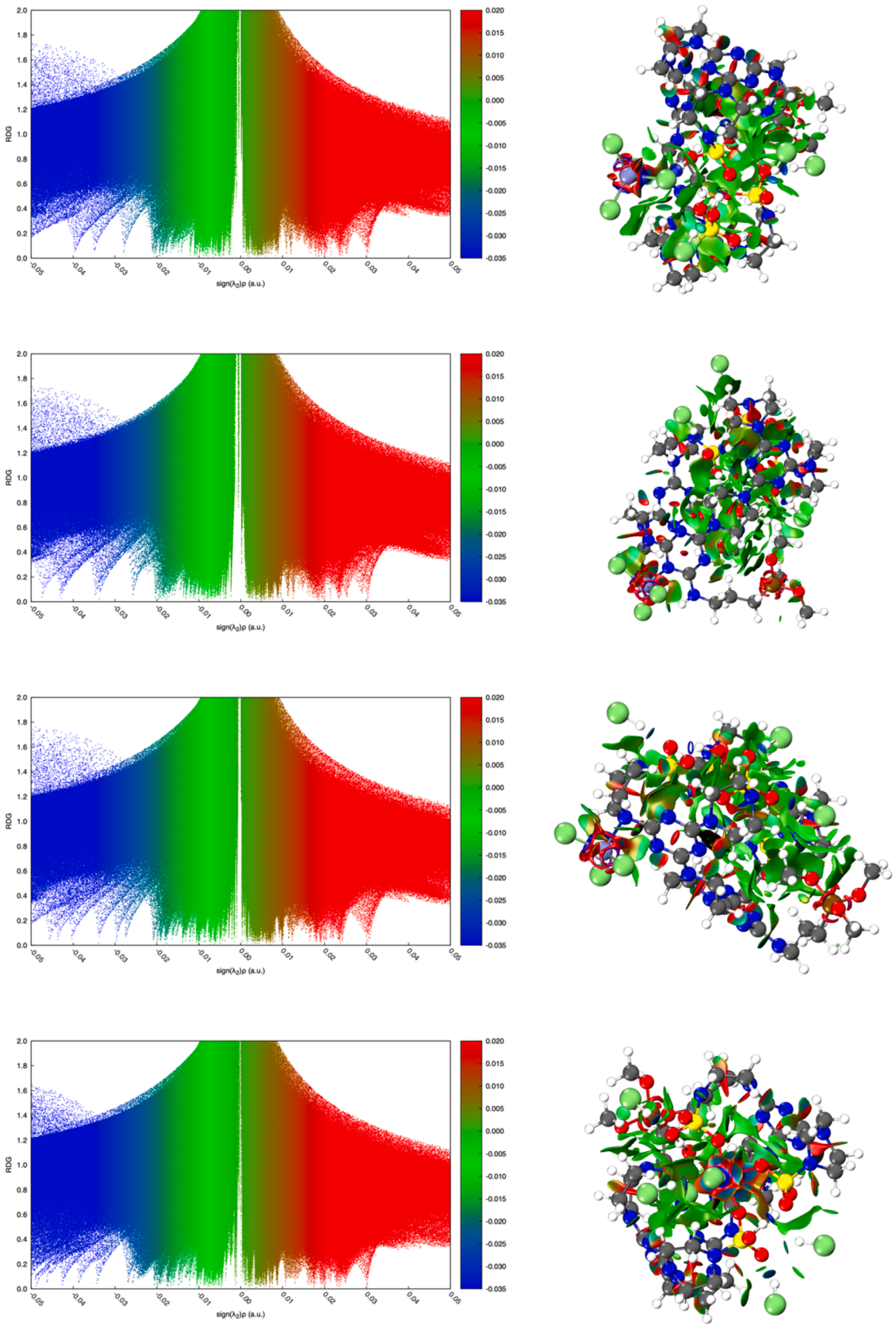

Fig. 11. 2D (left) and 3D (right) NCI plots of Gen2 and the addition of $AlCl_3$ on (a) Cl, (b) N of the aromatic ring, (c) non-aromatic N, and (d) the most accessible O atom of a SO_3 group.

demonstrating their effectiveness in the cationic polymerization of Raffinate-1 to produce conventional grade polybutenes. The incorporation of B-ILs into the $AlCl_3$ co-initiator system resulted in notable improvements in the polymerization process, including a reduction in the required amount of corrosive $AlCl_3$, thus enhancing safety and reducing costs.

Characterization techniques such as FTIR, TGA, SEM, and XRD confirmed the successful synthesis and integration of ILs onto the boehmite support, revealing the morphological and structural stability of the materials. The polymerization results indicated that the presence of B-ILs increased the molecular weight of the produced polybutenes and improved their viscosity characteristics, crucial for lubricant applications. The synthesized PBs exhibited desirable properties, such as high kinematic viscosity and viscosity index (VI), ensuring effective performance across a wide range of temperatures. DFT calculations contributed to the structural characterization of the interaction of the ionic liquids with the $AlCl_3$ moieties.

Overall, the study underscores the potential of advanced B-ILs in enhancing the efficiency and sustainability of lubricant production, paving the way for further innovations in the field. The use of ionic liquids, particularly those supported on boehmite, presents a promising approach to developing lubricants with superior performance and environmental benefits. Future research could focus on optimizing these materials and exploring their applications in other polymerization processes and industries.

CRediT authorship contribution statement

Amirhossein Ghavampoor: Writing – original draft, Investigation, Formal analysis, Data curation. **Naeimeh Bahri-Laleh:** Writing – review & editing, Investigation, Formal analysis, Data curation. **Samahe Sadjadi:** Writing – review & editing, Investigation, Formal analysis, Data curation. **Mehdi Nekoomanesh:** Investigation, Formal analysis, Data curation. **Amir Vahid:** Investigation, Formal analysis, Data curation. **Josep Duran:** Investigation, Formal analysis, Data curation. **Maciej Spiegel:** Writing – original draft, Investigation, Formal analysis, Data curation. **Albert Poater:** Writing – review & editing, Investigation, Formal analysis, Data curation.

Declaration of competing interest

The authors declare that they have no known competing financial interests or personal relationships that could have appeared to influence the work reported in this paper.

Data availability

The data are included in the Supporting Information and further details are available upon request, included in our own repositories.

Acknowledgment

The authors appreciate partial support of Iran Polymer and Petrochemical Institute. M.N is thankful to Iran National Science Foundation for financial support of the work under the grant number of 4023556. A. P. is a Serra Húnter Fellow and received ICREA Academia Prize 2019. We thank the Spanish Ministerio de Ciencia y Universidades (MICIU) for project PID2021-127423NB-I00 and the Generalitat de Catalunya for project 2021SGR623. The visit of Dr. Maciej Spiegel to the University of Girona was funded by Wroclaw Medical University (grant SUBK. D090.24.014). This research was carried out with the support of the Interdisciplinary Centre for Mathematical and Computational Modelling University of Warsaw (ICM UW) under computational allocation no G95-1798.

Appendix A. Supplementary material

Supplementary data to this article can be found online at https://doi.org/10.1016/j.molliq.2024.125814.

References

[1] R. Michalczewski, M. Kalbarczyk, A. Mankowska-Snopczynska, E. Osuch-Słomka, W. Piekoszewski, A. Snarski-Adamski, M. Szczerek, W. Tuszynski, J. Wulczynski, A. Wieczorek, The effect of a gear oil on abrasion, scuffing, and pitting of the DLC-coated 18CrNiMo7-6 steel, Coatings 9 (2018) 2.
[2] M. Sandomierski, T. Buchwald, A. Patalas, A. Voelkel, Improving the abrasion resistance of Ti_6Al_4V alloy by modifying its surface with a diazonium salt and attaching of polyurethane, Sci. Rep. 10 (2020) 19289.
[3] R. Kumar, I. Hussainova, R. Rahmani, M. Antonov, Solid lubrication at high-temperatures—a review, Materials 15 (2022) 1695.
[4] J.M. Martin, N. Ohmae, Colloidal lubrication: general principles, Nanolubricants (2008) 1–13.
[5] L. Rapoport, A. Moshkovich, V. Perfilyev, R. Tenne, On the efficacy of IF–WS 2 nanoparticles as solid lubricant: the effect of the loading scheme, Tribol. Lett. 28 (2007) 81–87.
[6] A. Zuin, T. Cousseau, A. Sinatora, S.H. Toma, K. Araki, H.E. Toma, Lipophilic magnetite nanoparticles coated with stearic acid: a potential agent for friction and wear reduction, Tribol. Int. 112 (2017) 10–19.
[7] S. Chen, T. Wu, C. Zhao, Conversion of lipid into high-viscosity branched bio-lubricant base oil, Green Chem. 22 (2020) 7348–7354.
[8] C. Chimeno-Trinchet, M.E. Pacheco, A. Fernández-González, M.E. Díaz-García, R. Badía-Laíño, New metal-free nanolubricants based on carbon-dots with outstanding antiwear performance, J. Ind. Eng. Chem. 87 (2020) 152–161.
[9] G. Biresaw, Biobased polyalphaolefin base oil: chemical, physical, and tribological properties, Tribol. Lett. 66 (2018) 1–16.
[10] Q. Zhang, B. Wu, R. Song, H. Song, J. Zhang, X. Hu, Preparation, characterization and tribological properties of polyalphaolefin with magnetic reduced graphene oxide/Fe_3O_4, Tribol. Int. 141 (2020) 105952.
[11] S.V. Kostjuk, Recent progress in the Lewis acid co-initiated cationic polymerization of isobutylene and 1,3-dienes, RSC Adv. 5 (2015) 13125–13144.
[12] A. Dedov, A.A. Karavaev, A.S. Loktev, A.K. Osipov, Bioisobutanol as a promising feedstock for production of "green" hydrocarbons and petrochemicals (a review), Petrol. Chem. 61 (2021) 1139–1157.
[13] L.R. Rudnick, Synthetics, Mineral Oils, and Bio-based Lubricants: Chemistry and Technology, CRC Press, 2020.
[14] R. Kumar, P. De, B. Zheng, K.-W. Huang, J. Emert, R. Faust, Synthesis of highly reactive polyisobutylene with $FeCl_3$/ether complexes in hexane; kinetic and mechanistic studies, Polym. Chem. 6 (2015) 322–329.
[15] I. Nifant'ev, S.A. Korchagina, M.S. Chinova, A.N. Tavtorkin, Polyisobutylenes with controlled molecular weight and chain-end structure: synthesis and actual applications, Polymers 15 (2023) 3415.
[16] B. Yang, R.F. Storey, Synthesis and characterization of polyisobutylene telechelic prepolymers with epoxide functionality, React. Funct. Polym. 150 (2020) 104563.
[17] W. Tomal, J. Ortyl, Water-soluble photoinitiators in biomedical applications, Polymers 12 (2020) 1073.
[18] H. Wang, S. Schilbach, M. Ninov, H. Urlaub, P. Cramer, Structures of transcription preinitiation complex engaged with the+ 1 nucleosome, Nat. Struct. Mol. Biol. 30 (2023) 226–232.
[19] G. Przesławski, K. Szczesniak, P. Gajewski, A. Marcinskowska, Influence of initiator concentration on the polymerization course of methacrylate bone cement, Polymers 14 (2022) 5005.
[20] J.B. Alves, M.K. Vasconcelos, L.H.R. Mangia, M. Tatagiba, J. Fidalgo, D. Campos, P. L. Invernici, M.V. Rebouças, M.H.S. Andrade, J.C. Pinto, A bibliometric survey on polyisobutylene manufacture, Processes 9 (2021) 1315.
[21] Y.-B. Jia, Y.-B. Wang, W.-M. Ren, T. Xu, J. Wang, X.-B. Lu, Mechanistic aspects of initiation and deactivation in N-heterocyclic olefin mediated polymerization of acrylates with alane as activator, Macromolecules 47 (2014) 1966–1972.
[22] P. Snetkov, K. Zakharova, S. Morozkina, R. Olekhnovich, M. Uspenskaya, Hyaluronic acid: The influence of molecular weight on structural, physical, physico-chemical, and degradable properties of biopolymer, Polymers 12 (2020) 1800.
[23] S. Yousefi, N. Bahri-Laleh, M. Nekoomanesh, M. Emami, S. Sadjadi, S. A. Mirmohammadi, M. Tomasini, E. Bardají, A. Poater, An efficient initiator system containing $AlCl_3$ and supported ionic-liquid for the synthesis of conventional grade polyisobutylene in mild conditions, J. Mol. Liq. 367 (2022) 120381.
[24] Q. Liu, Y.X. Wu, Y. Zhang, P.-F. Yan, R.-W. Xu, A cost-effective process for highly reactive polyisobutylenes via cationic polymerization coinitiated by $AlCl_3$, Polymer 51 (2010) 5960–5969.
[25] Z.I. Kahkeshi, M. Nekoomanesh-Haghighi, N. Bahri-Laleh, S. Sadjadi, Effect of support type on the characteristics of polybutene polymers from C4 monomers employing supported ionic liquid/$AlCl_3$ initiating systems, J. Mol. Struct. 1308 (2024) 138111.
[26] F. Karimi, M.A. Zolfigol, M. Yarie, A novel and reusable ionically tagged nanomagnetic catalyst: application for the preparation of 2-amino-6-(2-oxo-2H-chromen-3-yl)-4-arylnicotinonitriles via vinylogous anomeric based oxidation, Mol. Catal. 463 (2019) 20–29.

[27] A. Abo-Hamad, M.-A.-H. AlSaadi, M. Hayyan, I. Juneidi, M.A. Hashim, Ionic liquid-carbon nanomaterial hybrids for electrochemical sensor applications: a review, Electrochim. Acta 193 (2016) 321–343.

[28] M. Tabrizi, N. Bahri-Laleh, S. Sadjadi, M. Nekoomanesh-Haghighi, The effect of ionic liquid containing $AlCl_3$ catalytic systems on the microstructure and properties of polyalphaolefin based lubricants, J. Mol. Liq. 335 (2021) 116299.

[29] J. Choi, B. Nidetzky, Ionic liquid as dual-function catalyst and solvent for efficient synthesis of sucrose fatty acid esters, Mol. Catal. 526 (2022) 112371.

[30] M. Pashaei, E. Mehdipour, M. Azaroon, Engineered mesoporous ionic-modified γ-Fe_2O_3@ hydroxyapatite decorated with palladium nanoparticles and its catalytic properties in water, Appl. Organomet. Chem. 33 (2019) e4622.

[31] S. Sadjadi, F. Koohestani, G. Pareras, M. Nekoomanesh-Haghighi, N. Bahri-Laleh, A. Poater, Combined experimental and computational study on the role of ionic liquid containing ligand in the catalytic performance of halloysite-based hydrogenation catalyst, J. Mol. Liq. 331 (2021) 115740.

[32] I.V. Vasilenko, I.A. Berezianko, D.I. Shimana, S.V. Kostjuk, New catalysts for the synthesis of highly reactive polyisobutylene: chloroaluminate imidazole-based ionic liquids in the presence of diisopropyl ether, Polym. Chem. 7 (2021) 5615–5619.

[33] I.A. Berezianko, I.V. Vasilenko, S.V. Kostjuk, Silica gel supported ionic liquids as effective and reusable catalysts for the synthesis of highly reactive polyisobutylene in non-polar media, Polym. Chem. 13 (2022) 6625–6636.

[34] Z.I. Kahkeshi, N. Bahri-Laleh, S. Sadjadi, M. Nekoomanesh-Haghighi, An environmentally benign approach for the synthesis of low molar mass polybutenes from mixed C4 monomers using $AlCl_3$/ionic-liquid initiating systems, Mol. Catal. 547 (2023) 113332.

[35] S. Karthikeyan, V.K. Gupta, Highly reactive polyisobutylene through cationic polymerization of isobutylene, J. Polym. Res. 30 (2023) 337.

[36] M. Mashayekhi, S. Talebi, S. Sadjadi, N. Bahri-Laleh, Production of polyalfaolefin-based lubricants using new (poly) ionic liquid/$AlCl_3$ catalysts as environmentally friendly alternatives to commercial $AlCl_3$ route, Appl. Catal. A 623 (2021) 118274.

[37] S. Karimi, S. Sadjadi, N. Bahri-Laleh, M. Nekoomanesh-Haghighi, New less-toxic halloysite-supported ionic liquid/$AlCl_3$ oligomerization catalysts: a comparative study on the effects of various ionic liquids on the properties of polyalphaolefins, Mol. Catal. 509 (2021) 111648.

[38] S. Escayola, N. Bahri-Laleh, A. Poater, $\%V_{Bur}$ index and steric maps: from predictive catalysis to machine learning, Chem. Soc. Rev. 53 (2024) 853–882.

[39] R. Monreal-Corona, A. Pla-Quintana, A. Poater, Predictive catalysis: a valuable step towards machine learning, Trends Chem. 5 (2023) 935–946.

[40] R. Monreal-Corona, À. Díaz-Jiménez, A. Roglans, A. Poater, A. Pla-Quintana, Indolizine synthesis through annulation of pyridinium 1,4-thiolates and copper carbenes: a predictive catalysis approach, Adv. Synth. Catal. 365 (2023) 760–766.

[41] M.J. Frisch, G.W. Trucks, H.B. Schlegel, G.E. Scuseria, M.A. Robb, J.R. Cheeseman, G. Scalmani, V. Barone, G.A. Petersson, H. Nakatsuji, X. Li, M. Caricato, A. V. Marenich, J. Bloino, B.G. Janesko, R. Gomperts, B. Mennucci, H.P. Hratchian, J. V. Ortiz, A.F. Izmaylov, J.L. Sonnenberg, D. Williams-Young, F. Ding, F. Lipparini, F. Egidi, J. Goings, B. Peng, A. Petrone, T. Henderson, D. Ranasinghe, V. G. Zakrzewski, J. Gao, N. Rega, G. Zheng, W. Liang, M. Hada, M. Ehara, K. Toyota, R. Fukuda, J. Hasegawa, M. Ishida, T. Nakajima, Y. Honda, O. Kitao, H. Nakai, T. Vreven, K. Throssell, J.A. Montgomery Jr., J.E. Peralta, F. Ogliaro, M. J. Bearpark, J.J. Heyd, E.N. Brothers, K.N. Kudin, V.N. Staroverov, T.A. Keith, R. Kobayashi, J. Normand, K. Raghavachari, A.P. Rendell, J.C. Burant, S.S. Iyengar, J. Tomasi, M. Cossi, J.M. Millam, M. Klene, C. Adamo, R. Cammi, J.W. Ochterski, R.L. Martin, K. Morokuma, O. Farkas, J.B. Foresman, D.J. Fox, Gaussian 16, Revision C.01, Gaussian, Inc., Wallingford CT, 2016.

[42] A.D. Becke, Density-functional exchange-energy approximation with correct asymptotic behavior, Phys. Rev. A 38 (1988) 3098–3100.

[43] J.P. Perdew, Density-functional approximation for the correlation energy of the inhomogeneous electron gas, Phys. Rev. B 33 (1986) 8822–8824.

[44] S. Grimme, J. Antony, S. Ehrlich, H. Krieg, A consistent and accurate ab initio parametrization of density functional dispersion correction (DFT-D) for the 94 elements H-Pu, J. Chem. Phys. 132 (2010) 154104.

[45] F. Weigend, R. Ahlrichs, Balanced basis sets of split valence, triple zeta valence and quadruple zeta valence quality for H to Rn: design and assessment of accuracy, PCCP 7 (2005) 3297–3305.

[46] F. Weigend, Accurate Coulomb-fitting basis sets for H to Rn, PCCP 8 (2006) 1057–1065.

[47] A.D. Becke, Density-functional thermochemistry. III. The role of exact exchange, J. Chem. Phys. 98 (1993) 5648–5652.

[48] C. Lee, W. Yang, R.G. Parr, Development of the Colle-Salvetti correlation-energy formula into a functional of the electron density, Phys. Rev. B 37 (1988) 785–789.

[49] P.J. Stephens, F.J. Devlin, C.F. Chabalowski, M.J. Frisch, Ab initio calculation of vibrational absorption and circular dichroism spectra using density functional force fields, J. Phys. Chem. 98 (1994) 11623–11627.

[50] T.H. Dunning Jr, Gaussian basis sets for use in correlated molecular calculations. I. The atoms boron through neon and hydrogen, J. Chem. Phys. 90 (1989) 1007–1023.

[51] A.V. Marenich, C.J. Cramer, D.G. Truhlar, Universal solvation model based on solute electron density and on a continuum model of the solvent defined by the bulk dielectric constant and atomic surface tensions, J. Phys. Chem. B 113 (2009) 6378–6396.

[52] A. Ghorbani-Choghamarani, Z. Seydyosefi, B. Tahmasbi, Zirconium oxide complex anchored on boehmite nanoparticles as highly reusable organometallic catalyst for C-S and C–O coupling reactions, Appl. Organomet. Chem. 32 (2018) e4396.

[53] N.Y. Baran, T. Baran, M. Nasrollahzadeh, R.S. Varma, Pd nanoparticles stabilized on the Schiff base-modified boehmite: catalytic role in Suzuki coupling reaction and reduction of nitroarenes, J. Organomet. Chem. 900 (2019) 120916.

[54] S. Sadjadi, N. Abedian-Dehaghani, M.M. Heravi, Pd on cyclotriphosphazen-hexa imine decorated boehmite as an efficient catalyst for hydrogenation of nitro arenes under mild reaction condition, Sci. Rep. 12 (2022) 15040.

[55] T. Sun, Q. Zhuo, Y. Chen, Z. Wu, Synthesis of boehmite and its effect on flame retardancy of epoxy resin, High Perform. Polym. 27 (2015) 100–104.

[56] C. Liu, K. Shih, Y. Gao, F. Li, L. Wei, Dechlorinating transformation of propachlor through nucleophilic substitution by dithionite on the surface of alumina, J. Soil. Sediment. 12 (2012) 724–733.

[57] T.K. Vo, H.-K. Park, C.-W. Nam, S.-D. Kim, J. Kim, Facile synthesis and characterization of γ-AlOOH/PVA composite granules for Cr(VI) adsorption, J. Ind. Eng. Chem. 60 (2018) 485–492.

[58] S.-P. Lee, N. Mellon, A.M. Shariff, J.-M. Leveque, Aromatic polyamines covalent triazine polymer as sorbent for CO_2 adsorption. IOP Conference Series: Materials Science and Engineering, IOP Publishing, 2017.

[59] A. Jabbari, P. Moradi, M. Hajjami, B. Tahmasbi, Tetradentate copper complex supported on boehmite nanoparticles as an efficient and heterogeneous reusable nanocatalyst for the synthesis of diaryl ethers, Sci. Rep. 12 (2022) 11660.

[60] S. Karimi, N. Bahri-Laleh, S. Sadjadi, G. Pareras, M. Nekoomanesh-Haghighi, A. Poater, Pd on nitrogen rich polymer-halloysite nanocomposite as an environmentally benign and sustainable catalyst for hydrogenation of polyalfaolefin based lubricants, J. Ind. Eng. Chem. 97 (2021) 441–451.

[61] M. Tabrizi, S. Sadjadi, G. Pareras, M. Nekoomanesh-Haghighi, N. Bahri-Laleh, A. Poater, Efficient hydro-finishing of polyalfaolefin based lubricants under mild reaction condition using Pd on ligands decorated halloysite, J. Colloid Interface Sci. 581 (2021) 939–953.

[62] A. Shams, S. Sadjadi, J. Duran, S. Simon, A. Poater, N. Bahri-Laleh, Effect of support hydrophobicity of halloysite-based catalysts on the polyalphaolefin hydrofinishing performance, Appl. Organomet. Chem. 36 (2022) e6719.

[63] G. Zhu, L. Wang, J. Kuang, G. Xu, Y. Zhang, Q. Wang, High double bond content of polyisoprene synthesis via cationic polymerization synergistically catalyzed by Tf_2NH-ionic liquids, Macromolecules 54 (2021) 6109–6116.

[64] S. Nemes, J. Si, J.P. Kennedy, ^{13}C NMR chemical shifts of polyisobutylene end groups and related model compounds, Polym. Bull. 23 (1990) 597–603.

[65] L.-B. Zhang, Y.-X. Wu, P. Zhou, G.-Y. Wu, W.-T. Yang, D.-S. Yu, Synthesis of highly reactive polyisobutylenes with BF_3· cyclohexanol initiating system, Chin. J. Polym. Sci. 29 (2011) 360–367.

[66] L. Falivene, R. Credendino, A. Poater, A. Petta, L. Serra, R. Oliva, V. Scarano, L. Cavallo, SambVca 2. A web tool for analyzing catalytic pockets with topographic steric maps, Organometallics 35 (2016) 2286–2293.

[67] L. Falivene, Z. Cao, A. Petta, L. Serra, A. Poater, R. Oliva, V. Scarano, L. Cavallo, Towards the online computer-aided design of catalytic pockets, Nat. Chem. 11 (2019) 872–879.

[68] A. Poater, B. Cosenza, A. Correa, S. Giudice, F. Ragone, V. Scarano, L. Cavallo, SambVca: A web application for the calculation of buried volumes of N-heterocyclic carbene ligands, Eur. J. Inorg. Chem. 2009 (2009) 1759–1766.

[69] J. Bosson, A. Poater, L. Cavallo, S.P. Nolan, Mechanism of racemization of chiral alcohols mediated by 16-electron ruthenium complexes, J. Am. Chem. Soc. 132 (2010) 13146–13149.

[70] R. Mariz, A. Poater, M. Gatti, E. Drinkel, J.J. Bürgi, X. Luan, S. Blumentritt, A. Linden, L. Cavallo, R. Dorta, C2-symmetric chiral disulfoxide ligands in rhodium-catalyzed 1,4-addition: from ligand synthesis to the enantioselection pathway, Chem. Eur. J. 16 (2010) 14335–14347.

[71] A. Poater, F. Ragone, R. Mariz, R. Dorta, L. Cavallo, Comparing the enantioselective power of steric and electrostatic effects in transition-metal-catalyzed asymmetric synthesis, Chem. Eur. J. 16 (2010) 14348–14353.

[72] E.R. Johnson, S. Keinan, P. Mori-Sanchez, J. Contreras-Garcia, A.J. Cohen, W. T. Yang, Revealing noncovalent interactions, J. Am. Chem. Soc. 132 (2010) 6498–6506.

[73] J. Contreras-Garcia, E.R. Johnson, S. Keinan, R. Chaudret, J.P. Piquemal, D. N. Beratan, W.T. Yang, NCIPLOT: a program for plotting non-covalent interaction regions, J. Chem. Theory Comput. 7 (2011) 625–632.

[74] J. Contreras-García, R.A. Boto, F. Izquierdo-Ruiz, I. Reva, T. Woller, M. Alonso, A benchmark for the non-covalent interaction (NCI) index or… is it really all in the geometry? Theor. Chem. Acc. 135 (2016) 242.

[75] A. Shams, M. Mehdizadeh, H.-R. Teimoury, M. Emami, S.A. Mirmohammadi, S. Sadjadi, E. Bardají, A. Poater, N. Bahri-Laleh, Effect of the pore architecture of Ziegler-Natta catalyst on its behavior in propylene/1-hexene copolymerization, J. Ind. Eng. Chem. 116 (2022) 359–370.

[76] J. Poater, M. Gimferrer, A. Poater, Covalent and ionic capacity of MOFs to sorb small gas molecules, Inorg. Chem. 57 (2018) 6981–6990.

[77] R. Laplaza, F. Peccati, R.A. Boto, Y. Maday, J. Contreras-García, NCIPLOT and the analysis of noncovalent interactions using the reduced density gradient, Wiley Interdiscip. Rev.: Comput. Mol. Sci. 11 (2021) e1497.